


Structure-property relations of novel polyamide-6 elastomers prepared through reactive processing

Weibo Kong¹  · Yunyun Yang¹ · Zhimeng Liu¹ · Jingxin Lei¹

Received: 28 April 2017 / Accepted: 12 September 2017 / Published online: 26 September 2017
© Springer Science+Business Media B.V. 2017

Abstract A series of polyamide-6 elastomers (PAEs) employing polytetramethylene glycol (PTMG) as soft segments, diphenylmethane diisocyanate (MDI) as chain extender and polyamide-6 as hard segments is prepared through reactive processing. The MDI is also employed to suppress the crystallization capacity of soft segments and to regulate the soft segment length in the obtained PAEs. The chemical structures, crystallization properties, morphology, mechanical properties and thermal stability are extensively studied by Fourier transform infrared spectroscopy (FTIR), Hydrogen nuclear magnetic resonance (HNMR), X-ray diffraction (XRD), Differential scanning calorimetry (DSC), Transmission electron microscope (TEM), Dynamic mechanical analyzer (DMA), Tensile test and Thermal gravity analysis (TGA), respectively. TEM images demonstrate that PAE samples exhibit a microphase separated morphology with polyamide-6 domains disperse in the PTMG phase in nano-scale. DMA curves indicate that the prepared PAEs possess a typical elastomer thermodynamic behavior and a broad temperature-independent rubbery plateau. Meanwhile, PAEs exhibit superior mechanical properties with 55 MPa for tensile strength and 1100% for elongation at break. The TGA prove that the thermal stability of PAE can satisfy the requirement of multiple-processing without decomposition.

Keywords Thermoplastic elastomers · Reactive processing · Polyamide elastomers · Polyurethane

✉ Jingxin Lei
jxlei@scu.edu.cn

¹ State Key Laboratory of Polymer Materials Engineering, Polymer Research Institute of Sichuan University, No. 24, First South Section First Ring Road, Wuhou District, Chengdu 610065, China

Introduction

Thermoplastic elastomers (TPEs) are typical block copolymers consisting of two covalently linked segments (hard segments and soft segments) with different physical characteristics [1, 2]. The intermolecular interaction between the hard segments produce the physical crosslinking [3], which will impart TPEs with properties of chemically crosslinked rubbers as well as the good processability and moldability [4]. Meanwhile, the thermodynamic incompatibility of the hard and soft segments leads to the formation of a microphase separated morphology, which will generate the superior chemical and physical performance [5]. Therefore, TPEs have been employed to replace a large amount of materials in several commercial applications including advanced gas separation membranes, biomedical devices, food packaging, various textile modifiers, mechanical parts, construction materials, electronic equipment and automotive applications [6–10].

Polyamide elastomers (PAEs) are a sub-category of TPEs with polyamide as hard segments [10, 11]. Polyamide hard segments possess stronger intermolecular interaction and hydrogen bonding, which will enhance the mechanical properties, abrasion and solvent resistance and high temperature performance [9, 12, 13]. In addition, it is interesting and possible to tailor and prepare PAEs through the variation on the chemical structure and chain length of segments according to the practical application [14]. Many research have been conducted to prepare the PAE with different soft segments such as polycondensation of carboxylic acid terminated nylon oligomers with polytetramethylene glycol (PTMG) at high temperatures [15]; interesterification between diesters and diamines [16]; the polymerization between a dicarboxylic acid and diisocyanate [17] and so forth [18]. Our groups have synthesized a series of PAEs employing PTMG with different molecular weight as soft segment through reactive processing [11]. However, soft

segments with high molecular weight of PTMG ($M_w > 1000$) have strong crystallization capacity, which will cause an undesired effect on the low temperature performance and fracture toughness of PAEs. However, the high content of soft segments in PAEs is needed for improving the toughness, elasticity and low temperature performance in some case.

In this article, we report a promising strategy for producing a series of PAEs with different soft segment length by employing PTMG1000 as soft segment, MDI as chain extender and polyamide-6 as hard segment. MDI was employed to regulate the chain length of soft segments and suppress the crystallization of soft segment in the obtained PAEs. The obtained PAEs are extensively studied by Fourier transform infrared spectroscopy (FTIR), Hydrogen nuclear magnetic resonance (HNMR), X-ray diffraction (XRD), Differential scanning calorimetry (DSC), Transmission electron microscope (TEM), Dynamic mechanical analyzer (DMA) and Thermal gravity analysis (TGA).

Experimental

Materials

4, 4'-Diphenylmethane diisocyanate (MDI) was supplied by Yantai Wanhua polyurethane Co., Ltd. (Shandong, China). Polytetramethylene glycol (PTMG, $M_w = 1000$ g/mol) was purchased from Hyosung Chemicals Co., Ltd. (Jiaxing, China). The reagents above are used as received. α,ω -amino Polyamide-6 prepolymer (PA-6) with M_w of 1000 g/mol was prepared in the Lab.

Preparation of PAEs

PTMG1000 and MDI at a pre-determined ratio (Table 1) were putted into three neck flask equipped with thermometer and stirrer. The polymerization continued for 2.5 h under 80 °C. OPU-1, OPU-2 and OPU-3 represent the product with different molar ratio of PTMG/MDI as shown in Table 1. The dibutyl amine back titration method to determine the reaction end-point and molecular weight of OPU.

PA-6 powder was dried at 80 °C for 24 h under vacuum before blending with OPU at a molar ratio of 1:1. The polymerization was performed on HAAKE double-screw extruder (Thermo Scientific, America) at 130 rpm, and the temperature was set as 175 °C, 180 °C, 190 °C, 200 °C, 205 °C, 210 °C,

195 °C. The target materials were rushed into granules after cooling in water, and then dried in a vacuum oven at 80 °C. PAE-1, PAE-2 and PAE-3 represent the product with OPU-1, OPU-2 and OPU-3 as soft segments, respectively.

Characterization

FTIR

The chemical composition for each PAE was determined by FTIR- attenuated total reflectance (ATR) using Nicolet 170sx spectrometer (Thermo Nicolet Corporation, America) with a resolution setting of 4 cm^{-1} in a scanning range of 400–4000 cm^{-1} at room temperature.

HNMR

The chemical composition of PAEs was further calculated using the H-NMR, which was recorded on an INOVA-40 spectrometer (Varian Inc., Palo Alto, CA) at 400 Hz. For all PAEs samples, deuterated trifluoroacetic acid was used as a solvent.

DSC

The crystallization behaviors of PA-6 and obtained PAEs were studied by the DSC and the measurements were conducted on the thermal analysis instrument DSC 204 (NETZSCH, Germany). About 8 mg sample was loaded in an aluminum pan, and then sealed. All samples were heated from ambient temperature to 210 °C to erase any prior processing history of the samples. The temperature was then lowered to –30 °C. A second heating scan produced the DSC heating profile. Both heating and cooling temperature scans were carried out at the rate of 10 °C/min under a dry nitrogen atmosphere.

XRD

XRD measurements of PAEs films were conducted on high-resolution X-ray diffractometer (Phillips, Netherlands) in Bragg-Brentano geometry, using a Q compensating divergence slit (12.5 mm length). The testing was performed with a scanning rate of 2°/S with Cu K α radiation operating at 45kV and 40 ma within a scan range of $2\theta = 5 \sim 50^\circ/\text{S}$ at room temperature. The films prepared from a melt compression molded, subsequently, the films were heating at 20 °C/min to 200 °C. After that, the materials were cooled at 3 °C/min to ambient temperature, this special heat treatment was necessary to erase any effects generated by melting compression.

Table 1 The composition of OPU

	OPU-1	OPU-2	OPU-3
Molar ratio of PTMG1000 /MDI	1/2	2/3	3/4

TEM

For the TEM investigation, the copolymer was cooled to $-90\text{ }^{\circ}\text{C}$, subsequently, the sample was cut by a cryo ultramicrotomy on a Leica Ultracut-E cryo microtome with a diamond knife. The thin slice sample was collected by a carbon coated copper grid. TEM measurements were performed with Tecnai G2 F20 S-TWIN (FEI America) at an accelerating voltage of 200 kV.

DMA

The dynamic mechanical properties of PAEs were conducted on Q800 (TA Instruments, America) equipped with a liquid nitrogen cooling system under tensile mode. The samples were shaped into a rectangular shape ($15\text{ mm} \times 4\text{ mm} \times 2\text{ mm}$). The measurements were heated under a constant rate of $3\text{ }^{\circ}\text{C}/\text{min}$ over a temperature range of $-100\text{ }^{\circ}\text{C}$ to $180\text{ }^{\circ}\text{C}$ at a constant frequency of 1 Hz.

Tensile tests

The tensile tests for PAEs were carried out with an Instron-4302 Mechanical Tester (America) with a 1000 N load cell and a constant tensile rate of 500 mm min^{-1} . Dumbbell samples (neck part with $15\text{ mm} \times 4\text{ mm} \times 2\text{ mm}$) were prepared by an injection molding machine.

TGA

The thermal stability measurements of PAEs were performed on thermogravimetry-differential thermal analysis instrument SDT-Q600 (TA, America) in the temperature range of 30 to $600\text{ }^{\circ}\text{C}$ at a heating rate of $10\text{ }^{\circ}\text{C}/\text{min}$ under nitrogen. During the heating period, the weight loss and digital thermogravimetry were recorded as a function of temperature.

Results and discussion

FTIR

FTIR analysis was employed to study the chemical structure of each sample, and the FTIR curves are shown in Fig. 1. As for PA-6 (shown in Fig. 1a), the absorption at 3290 cm^{-1} and 1542 cm^{-1} are attributed to stretching vibration and bending vibration of $-\text{N}-\text{H}-$, and the absorption at 1640 cm^{-1} is recognized as characteristic peak of $\text{C}=\text{O}$ from amide groups. Besides, the two strong peaks at 2946 cm^{-1} and 2810 cm^{-1} are associated with $-\text{CH}_2-$. For OPU-1 in Fig. 1b, the peaks at 3291 cm^{-1} and 1550 cm^{-1} correspond to the stretching vibration and bending vibration of $-\text{N}-\text{H}-$ of urethane group, and the peak at 1750 cm^{-1} is ascribed to the $\text{C}=\text{O}$ stretching vibration

of urethane. Two distinct characteristic peaks at 2265 cm^{-1} and 1120 cm^{-1} are related with $-\text{NCO}$ and $-\text{C}-\text{O}-\text{C}-$. In addition, absorption peaks at 2946 cm^{-1} and 2810 cm^{-1} are assigned to $-\text{CH}_2-$ and $\text{C}-\text{H}$ stretching vibration. For prepared PAEs, each segment as well as chemical groups in PAE exhibits distinct peaks in the FTIR spectra. The peaks at 3301 cm^{-1} and 1550 cm^{-1} correspond to the stretching vibration and bending vibration of $-\text{N}-\text{H}-$ of amide and urethane, and peaks around 1750 cm^{-1} and 1230 cm^{-1} are assigned to the stretching vibration of $\text{C}=\text{O}$ and $-\text{C}-\text{O}-$ belong to urethane of OPU segments, respectively. PAEs possess the same absorption at 1640 cm^{-1} with PA-6, which is ascribed to the $\text{C}=\text{O}$ vibration of amide [19]. Moreover, all PAEs exhibit an ether peak at 1120 cm^{-1} as same as OPU [20]. It's worth noting that the characteristic signal of $-\text{CH}_2-$ belongs to PA-6 and OPU segments are overlap at 2694 cm^{-1} and 2810 cm^{-1} , meanwhile the disappearance of peak at 2265 cm^{-1} and the deterioration at 3290 cm^{-1} indicate the reaction occur between $-\text{NH}_2$ and $-\text{NCO}$. In addition, three PAEs demonstrate almost same the peak position but still exhibit distinct different about the intensity of those peaks, especially at 1120 cm^{-1} and 1640 cm^{-1} . With chain length increasing from OPU-1 to OPU-3, a dramatically increase is observed at the 1120 , 1230 and 1750 cm^{-1} peak with a simultaneous decrease in the 1640 , which are caused by the different OPU length in PAE-1, PAE-2 and PAE-3. As discussed above, the introduction of MDI extends the chain length of soft segments in PAE-2 and PAE-3.

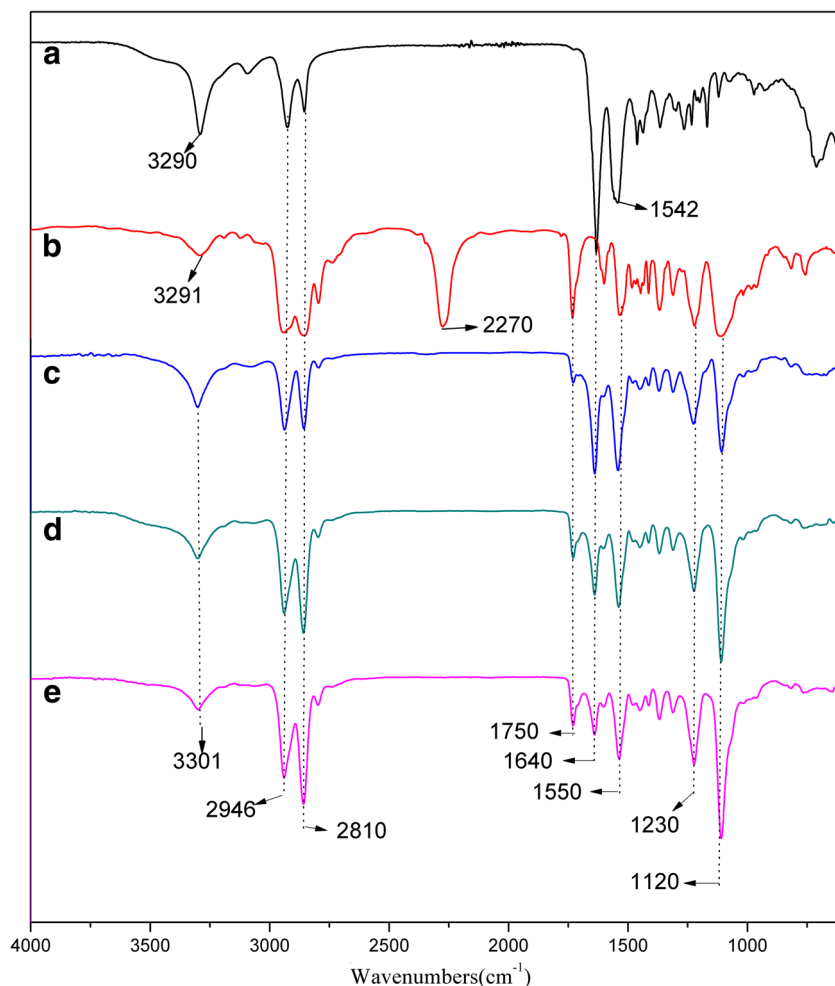
HNMR

The chemical structures of PAEs can be specified more quantitatively by HNMR analysis and HNMR spectra of PAEs are shown in Fig. 2. Three PAEs have similar HNMR curves, indicating the analogical chemical structure of prepared PAEs. H signals around $\delta 6.34$ are characteristic for benzene ring in MDI and the five methylene groups in PA-6 exhibit peaks at $\delta 0.65$, 1.16 , 1.88 , 2.71 , 3.11 , respectively. Meanwhile, the HNMR spectra of PAEs display two sharp peaks at $\delta 2.9$ and 0.8 , which are attributed to the protons in PTMG. From the results of FTIR and HNMR, it can draw conclusion that PAEs with PA-6 as hard segments, PTMG as soft segments and MDI as coupling agent are obtained.

DSC

The crystalline properties are important parameters for the PAEs, so the crystalline properties of PAEs are investigated by the DSC and XRD. The cooling and heating thermal scans of DSC results are distinctly shown in Fig. 3a and b, respectively. In the cooling scan, an exothermic peak appears around $-20\text{ }^{\circ}\text{C}$ for PAE-1 which is caused by the crystallization behaviors of the PTMG1000 segments. However, the

Fig. 1 The FTIR spectra of samples. a: PA-6; b: OPU-1; c: PAE-1; d: PAE-2; e: PAE-3



amount of PTMG segments crystallinity reflected by the ΔH_c is low, and this result could be related to the short PTMG segments are not easy to form crystalline domains. As for

PAE-2 and PAE-3, no exothermic peak is detected around $-20\text{ }^\circ\text{C}$ in cooling scan, which means that there is no crystallization of PTMG segments in PAE-2 and PAE-3. This phenomenon must be due to the introduction of MDI into OPU, and with the increasing amount of MDI in OPU, the destruction degree of the regularity and flexibility of PTMG segments increase. In addition, the PA-6 exhibit an exothermic peak at $140\text{ }^\circ\text{C}$, suggesting that the crystalline growth velocity of PA-6 segments are too low to be detected under this testing condition [21].

The heating scans of PAEs are shown in Fig. 3b. PAE-1 has an endothermic peak around the $9\text{ }^\circ\text{C}$ corresponding to the melting of PTMG1000 crystal. On the contrary, PAE-2 and PAE-3 exhibit no transition around $9\text{ }^\circ\text{C}$, which is ascribed from the inability of PTMG chain to develop lamellae crystals. In addition, PAE-1 demonstrates a slight endothermic peak around $165\text{ }^\circ\text{C}$ similar to the PA-6, however PAE-2 and PAE-3 do not, such observation is attributed to the stronger solvation of OPU-2 and OPU-3 soft segments [22]. In conclusion, the introduction of MDI into soft segments can restrain the crystallization capacity of PTMG especially for PAE-2 and PAE-3.

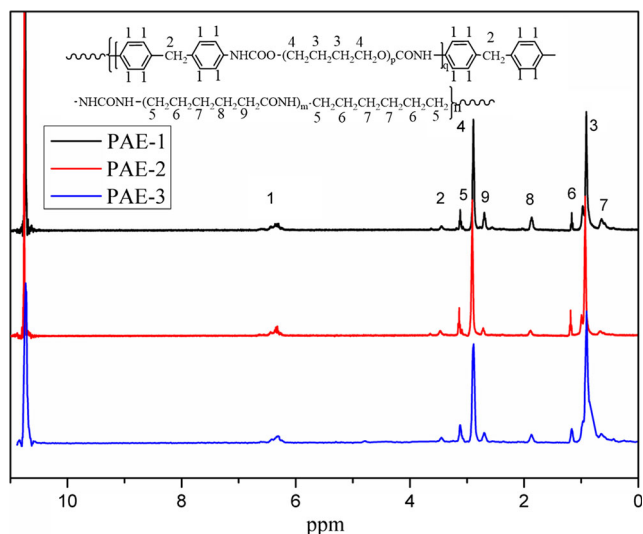


Fig. 2 The ^1H NMR spectra of obtained PAEs

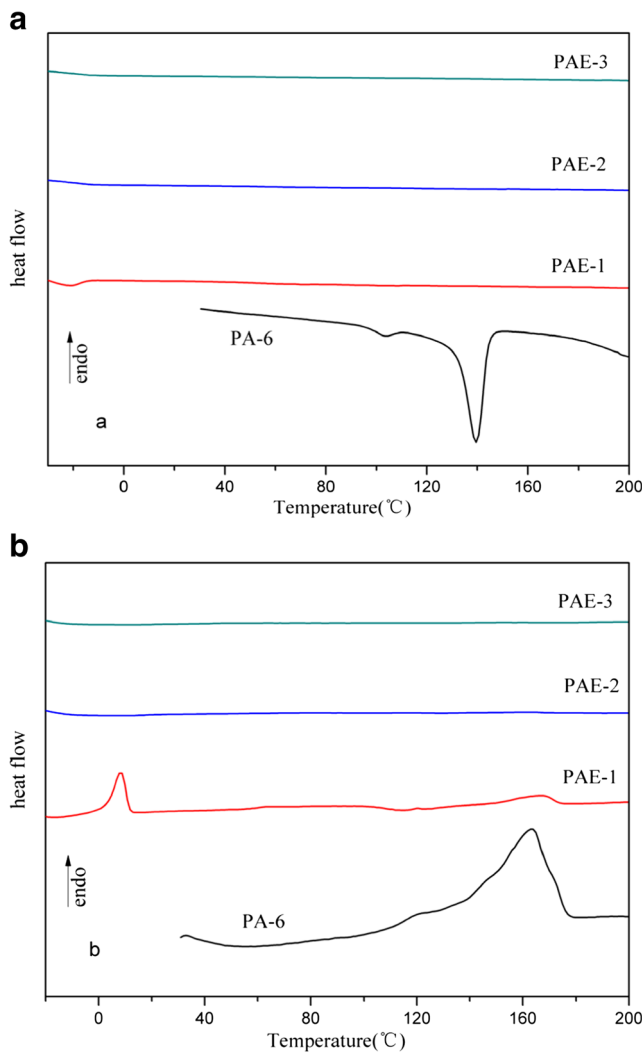


Fig. 3 DSC spectra of PAEs, **a**: the cooling scan; **b**: the heating scan

XRD

XRD was employed to further study the crystalline structure of PAEs. As shown in Fig. 4, PAEs with crystalline PA-6 segments exhibit a broad and weak peak at 2θ -values of 40° in XRD curves. The low scattering intensity of PA-6 crystallites can be explained by the fact that the soft segments in PAE backbone may destroy the neat structure of PA-6 segment [23]. A broad and strong peak around 20° is ascribed to the amorphous PTMG phase in PAEs (the testing is conducted at 25°C , so PTMG in PAE-1 is amorphous) [24], and the characteristic diffraction sharp peak of crystalline PTMG phase is not detected. XRD results indicated that the PTMG soft segments are amorphous, which is consistent with the DSC results. In addition, the crystalline hard segments coupled with the amorphous soft segments are favorable to form the microphase separated morphology in PAEs.

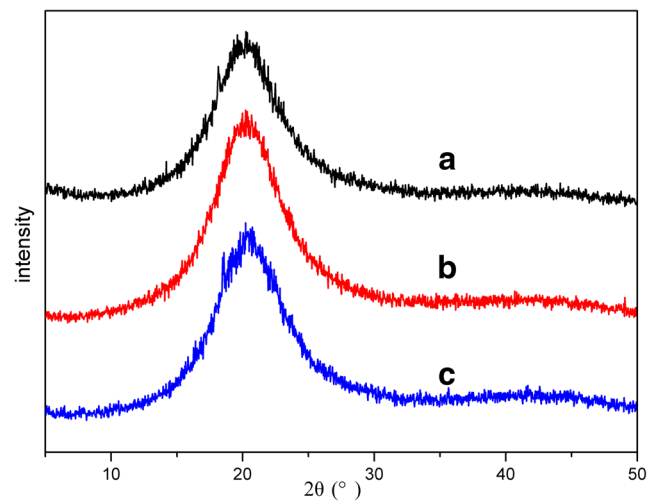


Fig. 4 The wide-angle X-ray diffraction spectra of **a**: PAE-1; **b**: PAE-2; **c**: PAE-3

TEM

The microphase separation is caused by the incompatibility of the hard and soft segments that give rise to superior properties of PAEs. The morphology of PAEs is extensively investigated by TEM and the TEM images are shown in Fig. 5. The hard segment domains, function as the physical crosslinks in PAEs, will enhance the physical and chemical properties of PAEs. For PAE-1, shown in Fig. 5a, the spherical domains with a diameter of approximately 120 nm are dispersed in the matrix, which suggests a high degree of microphase separation between hard segments and soft segments. In addition, some other irregular domains are also observed in the TEM image of PAE-1. As for PAE-2, one large domain with diameter of approximately 300 nm along with many small irregular domains with uneven size are dispersed in soft segments, which indicate a slight lower degree microphase separated of PAE-2 compared with PAE-1. The large domains may be caused by the overlap of PA-6 hard segments domains. As for PAE-3, only two domains with diameter of approximately 150 nm come into view in Fig. 5c, which shows that PAE-3 has the minimum degree of microphase separation in the three PAEs. It is worthy to note that uniformity and number of hard segments domains decrease with the increasing of the OPU length from PAE-1 to PAE-3. The PAE-2 and PAE-3 have less hard segments domains must be due to the less PA-6 segments content and stronger solvation of PTMG [25]. Meanwhile, PAE-2 and PAE-3 have larger number of urethane groups due to the introduction of MDI. The urethane groups will improve the intermolecular force between soft and hard segment, which is harmful to the microphase separated between two segments. Even so, the dispersion of hard segments domains in soft segments is observed in PAEs, which proves the good microphase separated morphology in PAEs [26].

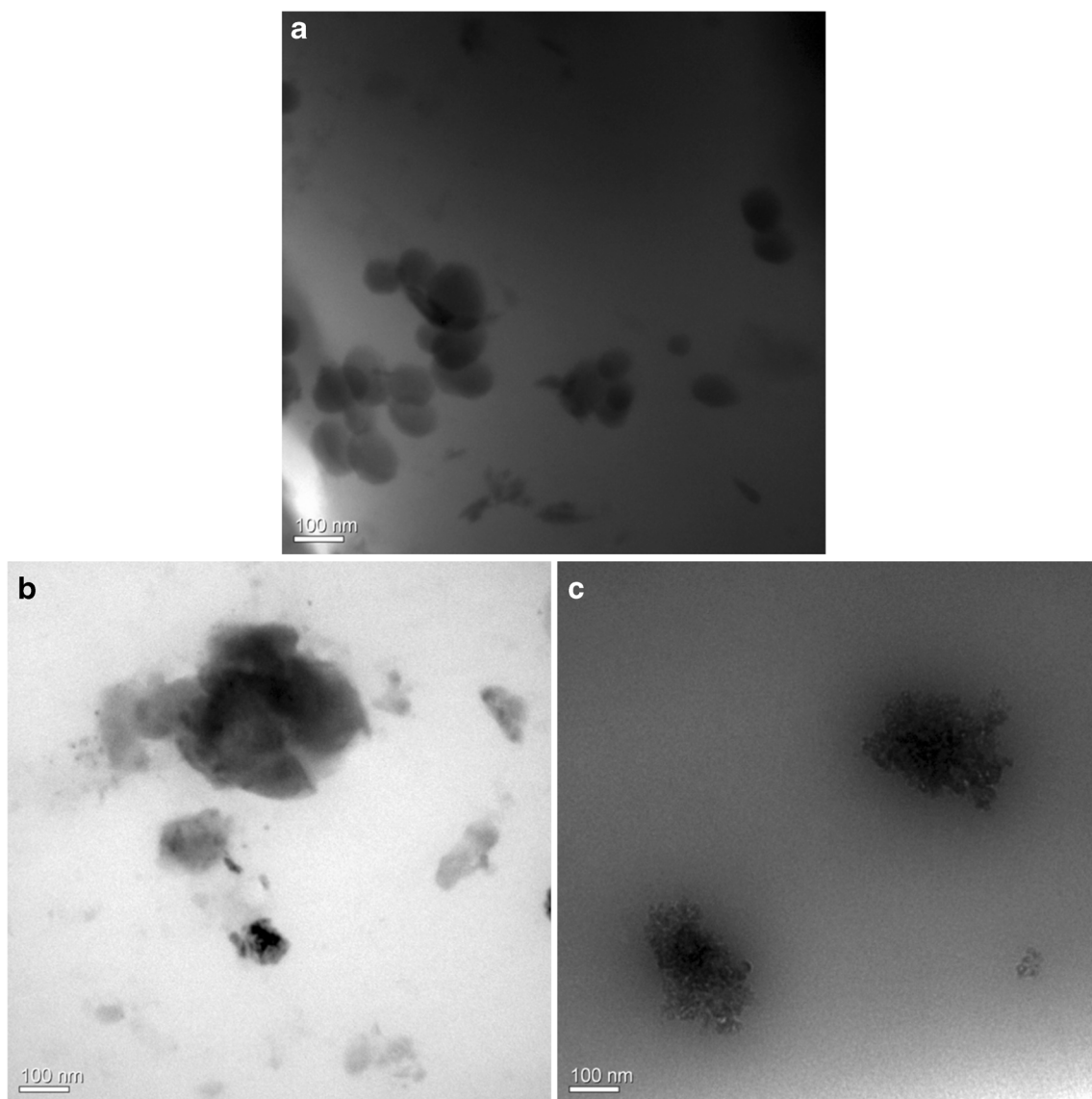


Fig. 5 The morphology images of the **a:** PAE-1; **b:** PAE-2; **c:** PAE-3

DMA

PAEs were extensively studied by DMA, and G' , G'' and loss factor were recorded as a function of temperature. As shown in Fig. 6a, in brief, the G' behavior tends to display three particular regions despite there are some additional subtleties. In the range of -100 to -70 °C, PAEs are glassy and have G' value of about 3GPa. PAE-1 exhibits a higher G' than PAE-2 and PAE-3 in this temperature range, which is attributed from the higher PA-6 content in PAE-1. Beginning at -70 °C, each PAE exhibits a drop of G' which is caused by the glass transition of the PTMG amorphous phase. Just as one expected, the transition is more particularly distinct for PAE-2 and PAE-3 with higher PTMG content. After this transition, PAE-2 and PAE-3 possesses similar temperature independent rubbery plateau which arises from the appropriate microphase separation. The rubbery plateau

range extends from the order of -25 to 125 °C, and the broader rubbery plateau could make PAE-2 and PAE-3 interesting for many practical applications. Following the rubbery plateau region, there demonstrate a drop of G' that corresponds to the softening of PA-6 hard segments. Moreover, the onset temperature of G' declines decrease with the decreasing of PA-6 content from PAE-1 to PAE-3. Further supports for the above points can be seen from Fig. 6b, the G'' curves of PAEs exhibit one peak at -60 °C followed by a shoulder at about 30 °C. The maximum peak corresponds to the T_g of the PTMG amorphous phase and the relaxation at 30 °C should attribute by the T_g of the PA-6 amorphous phase. In addition, the sharp peaks of G'' at T_g suggest good microphase separation morphology in PAEs. In addition, the introduction of MDI eliminates characteristic peak assigned to the melting of long PTMG chain, which was detected in the previous research [11].

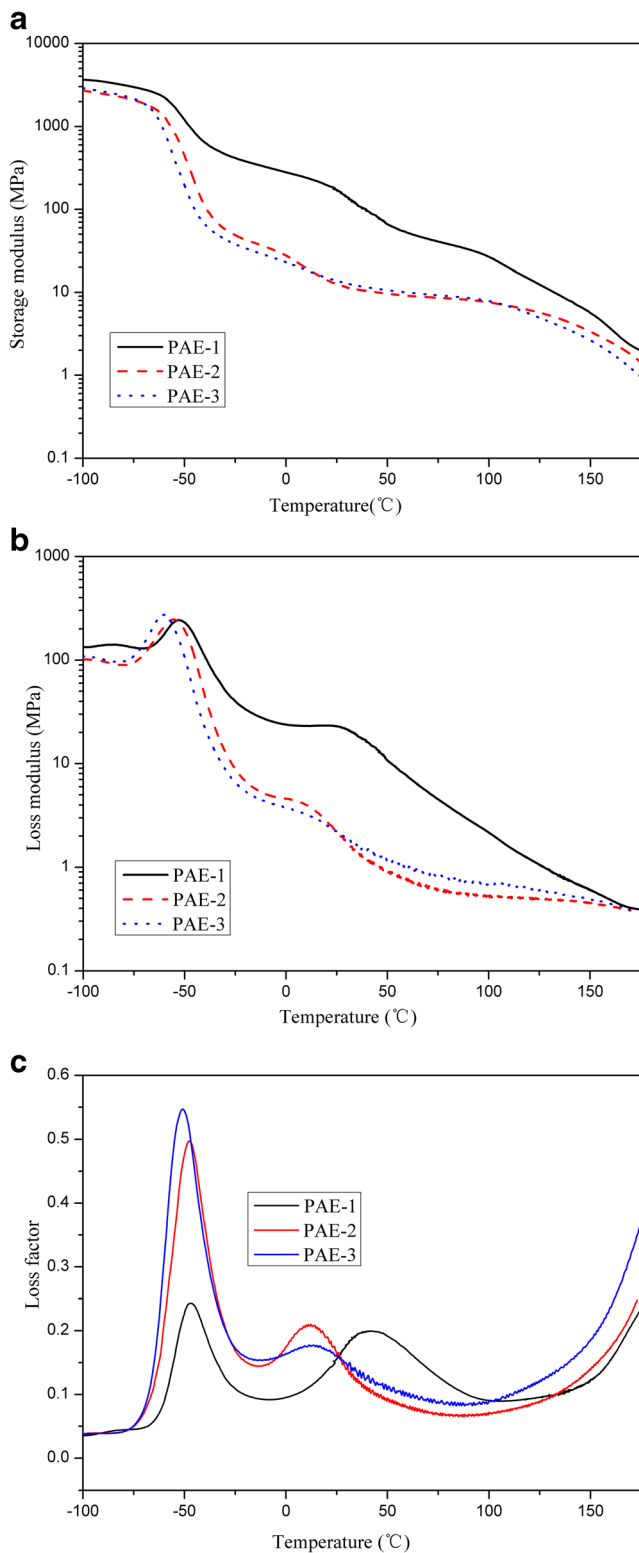


Fig. 6 DMA results of obtained PAEs. **a:** storage modulus (G') of PAEs, **b:** loss modulus (G'') of PAEs, **c:** loss factor of PAEs

The Loss factor provides further information about the dynamic mechanical behavior of the PAEs. As is clearly visible in Fig. 6c, the curves display two distinct transitions that are in

good accordance with the G'' dates. In the temperature range of -100 to -70 °C, PAEs demonstrate no change because of the molecular chain has only the local motion of methylene sequence [27]. Turning attention to the damping increase at -50 °C, this distinct peak is caused by the PTMG glass transition as confirmed by many segment polymers with PTMG as soft segment. Moreover, the magnitude of this peak is consistent with the PTMG content in PAEs. One note that, there is no obvious peak in the range of -20 to 20 °C which stems from the melting of PTMG, suggesting that regularity and flexibility of PTMG molecular chain have been destroyed by MDI. The peaks around the 20 – 50 °C are obvious the glass transition of PA-6. It is worth noting that this peak becomes more distinct and move to higher temperature as the PA-6 content increase. Finally, the rise in loss factor around 160 °C is simply caused by melting of the PA-6 crystal which have been addressed when discussing G' . In addition, the distance between two T_g can be used to evaluate the degree of microphase separation, from this the degree of microphase separated decreases in order: PAE-1 > PAE-2 > PAE-3, which is consistent with the results of TEM.

Tensile testing

Tensile testing provides extremely important parameters for evaluating the performance and application of polymer. The stress versus strain curves of PAEs are clearly shown in Fig. 7. PAEs exhibit a remarkably high elongation at break and low Young's modulus without distinct yield point, indicative of an elastomeric behavior. The Young's modulus decreases linearly with the decreasing of PA-6 segments content. PAE-2 demonstrates an excellent mechanical property with tensile strength exceeds 55 MPa and the elongation at break exceeds 1100%, this must be due to the microphase separated phase of hard and soft segments and the strong intermolecular forces. The area under the stress-strain curve can be used to evaluate the

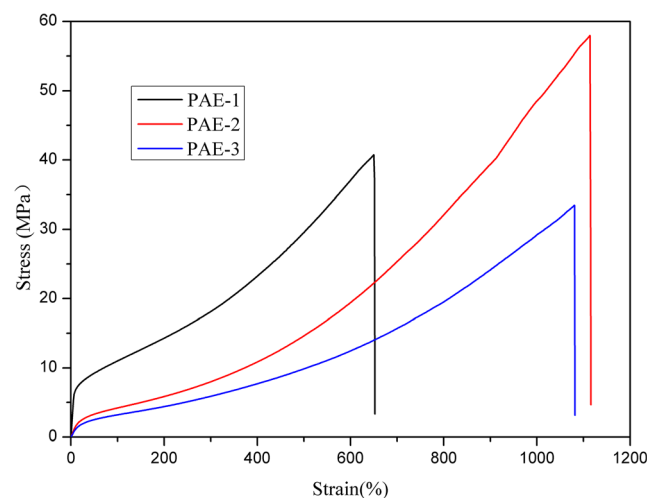


Fig. 7 Mechanical properties of obtained PAEs

toughness of the material, and under these measuring standard, PAE-2 is the toughest material within the series. As for PAE-3, the mechanical properties are inferior to PAE-2, which must arise from the extremely low PA-6 segments content.

TGA

The TGA was used to study the thermal stability of PAEs, and TG and DTG results are shown in Fig. 8a and b, respectively. The thermal stability parameters corresponding to these PAEs with the different structure are given in Table 2. As shown in Fig. 8a, All PAEs display similar degradation profiles of a slow initial and then a more rapid degradation process, suggesting a two-step mechanism for the degradation, as is evident from DTG curves in Fig. 8b [28]. From TGA curves, it is found that onset degradation temperature (T_{on}) for PAEs is high (above 300 °C), indicating that they are reasonably stable up to their melting point. This must be attributed to the thermostability of

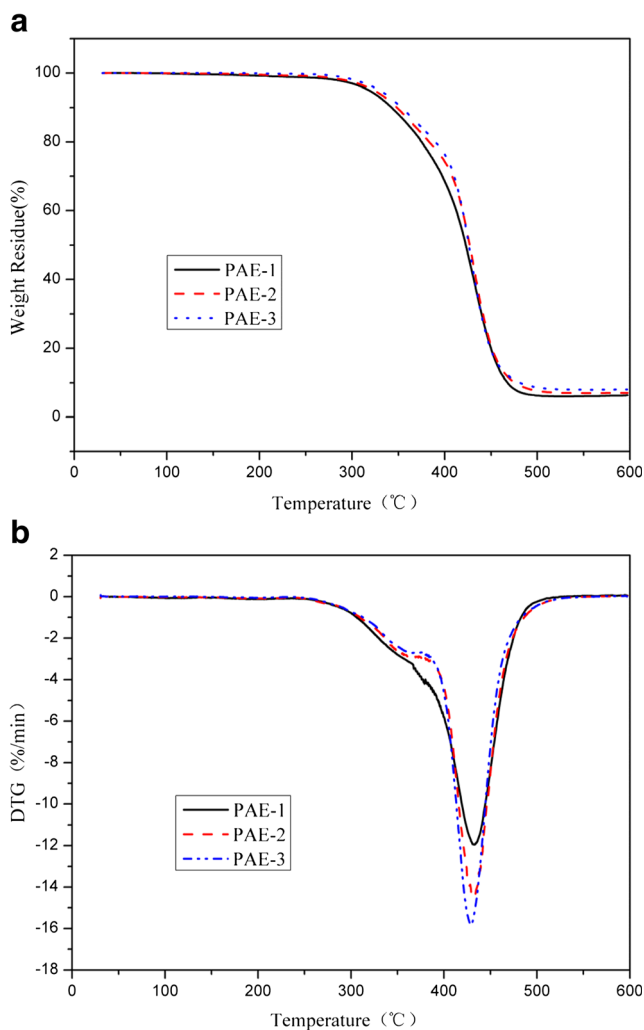


Fig. 8 Thermal stability of the obtained PAEs. **a:** TGA curves of PAEs; **b:** DTG curves of PAEs

Table 2 Characteristic temperature on TGA curves

PAE	T_{on} (°C)	$T_{10\%}$ (°C)	DTG peak (°C)	
			T_{1m}^a	T_{2m}^b
PAE-1	301.0	342.9	345.7	433.0
PAE-2	305.2	348.5	352.2	432.1
PAE-3	311.6	353.5	360.3	429.6

^a T_{1m} means the first DTG peak in Fig. 8b

^b T_{2m} means the second DTG peak in Fig. 8b

PA-6 segments in PAEs, meanwhile it has been proven previously that the urea and urethane groups may behave as antioxidant and have a stabilizing effect on the soft segment [28]. In addition, the strong hydrogen bonding between the PA-6 segments and urethane also favor to the thermal stability of PAEs. In contrast, the temperature stability is decreasing in the order: PAE-3 > PAE-2 > PAE-1, if the criteria for stability are taken as the temperature at which 10% weight loss occurred ($T_{10\%}$), the same conclusion can be reached. It may be caused by the fact that: PAE-3 has a low degree microphase phase separation. At high temperature (above 300 °C), the hydrogen bonding dissociated hence the protection function of PA-6 segments play a major role in the thermal stability of PAEs. The protection function of PA-6 segments increase with the decreasing of microphase separated degree in PAEs. Therefore, the temperature at T_{on} and $T_{10\%}$ weight loss for PAE-3 is higher than that of PAE-1 and PAE-2.

Conclusion

The expected property outcome was achieved from the PAEs using the reactive processing approach within this study. Moreover, the introduction of MDI in soft segments, functioned as crystallization inhibitor, successfully suppressed the crystallization capacity of PTMG. The FTIR results showed the successfully preparation of PAEs through reactive processing. DSC and XRD results suggested that the crystallization capacity of PTMG was restricted, and the crystallization of hard segments is slow. The TEM images demonstrated the evidently microphase separation morphology of PAEs with the PA-6 domains dispersed in the soft segments matrix. And the amount of hard segment domains increases with the increasing of PA-6 content. The storage modulus showed that PAE-2 and PAE-3 exhibit a broad temperature-independent rubbery plateau in the temperature range of -20 – 150 °C and all PAEs demonstrated two T_g which proves a good microphase separation morphology consistent with TEM results. The tensile test demonstrated the excellent mechanical properties of prepared PAEs, especially for PAE-2. The TGA results

indicated that the PAEs have a good thermal stability and can be fabricated without any decomposition as long as the temperature does not exceed 300 °C. The microphase separated degree of PAEs can be tuned by changing the structure and content of two segments in PAEs.

Compliance with ethical standards

Conflict of interest We declare that we have no financial and personal relationships with other people or organizations that can inappropriately influence our work, there is no professional or other personal interest of any nature or kind in any product, service and/or company that could be construed as influencing the position presented in, or the review of, the manuscript entitled “Structure-property relations of novel polyamide-6 elastomers prepared through reactive processing”.

References

- Li S, Sang Z, Zhao J, Zhang Z, Cheng J, Zhang J (2016) Synthesis and properties of non-isocyanate aliphatic crystallizable thermoplastic poly(ether urethane) elastomers. *Eur Polym J* 84:784–798
- Jung HS, Choi MC, Chang Y, Kang P, Hong SC (2015) Facile preparation of thermoplastic elastomer with high service temperature from dry selective curing of compatibilized EPDM/polyamide-12 blends. *Eur Polym J* 66:367–375
- Castagna AM, Pango A, Choi T, Dillon GP, Runt J (2012) The role of soft segment molecular weight on microphase separation and dynamics of bulk polymerized polyureas. *Macromolecules* 45(20):8438–8444
- Gonzalez I, Ignacio Eguiazabal J, Nazabal J (2012) Amorphous polyamide/maleated styrene-ethylene-co-butylene-styrene nanocomposites: effects of clay loading and compatibilizer content on morphology and mechanical properties. *Polym J* 44(3):294–300
- Ten Cate AT, Sijbesma RP (2002) Coils, rods and rings in hydrogen-bonded supramolecular polymers. *Macromol Rapid Commun* 23(18):1094–1112
- Okoroafor E, Rault J (1991) Cryodilation of thermoplastic peba elastomers. *J Polym Sci Polym Phys* 29(11):1427–1436
- Choi M, Jung J, Yeom H, Chang Y (2013) Mechanical, thermal, barrier, and rheological properties of poly(ether-block-amide) elastomer/organoclay nanocomposite prepared by melt blending. *Polym Eng Sci* 53(5):982–991
- Huo L, Li H (2012) Synthesis of segmented block copolymers based on polyamide-1010 and polytetramethylene glycol. *Adv Mater Res* 512-515:2185–2190
- Wang Y, Alhassan SM, Yang VH, Schiraldi DA (2013) Polyether-block-amide copolymer/clay films prepared via a freeze-drying method. *Compos Part B* 45(1):625–630
- Buckwalter DJ, Dennis JM, Long TE (2015) Amide-containing segmented copolymers. *Prog Polym Sci* 45:1–22
- Kong W, Yang Y, Liu Z, Jiang L, Zhou C, Lei J (2016) Structure-property relations of nylon-6 and polytetramethylene glycol based multiblock copolymers with microphase separation prepared through reactive processing. *Polym Int*
- Kim JH, Ha SY, Lee YM (2001) Gas permeation of poly(amide-6-b-ethylene oxide) copolymer. *J Membr Sci* 190(2):179–193
- Tavernier B, Mewis J, Van Puyvelde P, Takenaka M, Ernst B, Hashimoto T (2008) Effect of thermomechanical history on the crystallization of poly(ether-block-amide). *Polym Eng Sci* 48(12):2418–2425
- Sheth JP, Klinedinst DB, Wilkes GL, Yilgor I, Yilgor E (2005) Role of chain symmetry and hydrogen bonding in segmented copolymers with monodisperse hard segments. *Polymer* 46(18):7317–7322
- Mallakpour S, Kowsari E (2006) Polycondensation reaction of N,N'-(4,4'-oxydipthaloyl)-bis-L-methionine diacid chloride with aromatic diamines: synthesis and properties. *J Appl Polym Sci* 99(3):1038–1044
- Poullès F, Mouysset D, Gil G, Bertrand MP, Gastaldi S (2012) Novozym 435-catalyzed synthesis of polyetheramides from amino-esters, or diesters and diamines built on ethylene- and diethylene-glycol moieties. *Polymer* 53(6):1172–1179
- Yi C, Peng Z, Wang H, Li M, Wang C (2011) Synthesis and characteristics of thermoplastic elastomer based on polyamide-6. *Polym Int* 60(12):1728–1736
- Boulares A, Tessier M, Maréchal E (2000) Synthesis and characterization of poly(copolyethers-block-polyamides) II. Characterization and properties of the multiblock copolymers. *Polymer* 41(10):3561–3580
- McCarthy SJ, Meijs GF, Mitchell N, Gunatillake PA, Heath G, Brandwood A, Schindhelm K (1997) In-vivo degradation of polyurethanes: transmission-FTIR microscopic characterization of polyurethanes sectioned by cryomicrotomy. *Biomaterials* 18(21):1387–1409
- Upadhyay DJ, Cui N, Anderson CA, Brown NMD (2004) A comparative study of the surface activation of polyamides using an air dielectric barrier discharge. *Colloids Surf A Physicochem Eng Asp* 248(1–3):47–56
- Nielsen MCEJ, Feijen J, Gaymans RJ (2000) Synthesis and properties of segmented copolymers having aramid units of uniform length. *Polymer* 41(24):8487–8500
- van der Schuur M, Gaymans RJ (2006) Segmented block copolymers based on poly(propylene oxide) and monodisperse polyamide-6, T segments. *J Polym Sci A Polym Chem* 44(16):4769–4781
- Nielsen MCEJ, Harkema S, van der Heide E, Gaymans RJ (2001) Structural changes of segmented copolyetheresteramides with uniform aramid units induced by melting and deformation. *Polymer* 42(3):1131–1142
- Peyravi M, Babaluo AA, Ardestani MA, Aghjeh MKR, Pishghadam SR, Hadi P (2010) Study on the synthesis of poly(ether-block-amide) copolymer based on nylon6 and poly(ethylene oxide) with various block lengths. *J Appl Polym Sci* 118(2):1211–1218
- Helfand E, Lauritzen JJ (1973) Theory of copolymer crystallization. *Macromolecules* 6(4):631–638
- Zhang S, Wang G, Jiang Z, Wang D, Ma R, Wu Z (2005) Impact properties, phase structure, compatibility, and fracture morphology of polyamide-1010/thermoplastic poly(ester urethane) elastomer blends. *J Polym Sci B Polym Phys* 43(10):1177–1185
- Boublil H, Okoroafor E, Belhoucine M, Rault J, Glotin M (1989) Morphology of polyamide and polyether block amide blends. *Polym Eng Sci* 29(10):679–684
- Wang T, Hsieh T (1997) Effect of polyol structure and molecular weight on the thermal stability of segmented poly(urethaneureas). *Polym Degrad Stab* 55(1):95–102